Clinical Pediatric Endocrinology

Vol.34 / No.2
April 2025
pp 89–104

Review

Imaging findings of thyroid diseases in children

Yuko Tsujioka[1], Yoshitake Yamada[1], Tomonobu Hasegawa[2], Masahiro Hashimoto[1], and Masahiro Jinzaki[1]

[1]*Department of Radiology, Keio University School of Medicine, Tokyo, Japan*
[2]*Department of Pediatrics, Keio University School of Medicine, Tokyo, Japan*

Highlights

- We reviewed the imaging findings in pediatric thyroid diseases.
- Ultrasonography plays a central role in the diagnosis of this group of disorders.
- Scintigraphy can provide functional implication for thyroid dyshormogenesis.

Abstract. We review the imaging findings in pediatric thyroid diseases that necessitate prompt diagnosis and timely medical intervention. Congenital hypothyroidism particularly represents a critical pediatric emergency. Ultrasonography stands as the primary modality for accurately assessing thyroid morphology and identifying thyroid dysgenesis. ^{123}I-scintigraphy mirrors iodine metabolism and thyroid hormone synthesis, and the concurrent application of perchlorate (perchloride discharge test) elucidates the pathogenesis of thyroid dyshormonogenesis. Nonetheless, radioiodine scintigraphy has seen limited utilization due to the intricacies of pre-test preparation. ^{99m}Tc-pertechnetate scintigraphy demonstrates high sensitivity in delineating thyroid tissues with minimal radiation exposure, facilitating the diagnosis of thyroid dysgenesis. Additionally, we have included brief insights on the imaging characteristics of central hypothyroidism, thyroiditis, and thyroid masses.

Key words: pediatric thyroid disease, thyroid dysgenesis, thyroid dyshormogenesis, thyroiditis, thyroid imaging

Received: November 1, 2024 Accepted: January 8, 2025 Advanced Epub: January 30, 2025
Corresponding author: Yuko Tsujioka, Department of Radiology, Keio University School of Medicine, 35 Shinanomachi, Shinjuku-ku, Tokyo 160-0016, Japan
E-mail: yuko.tsujioka@rad.med.keio.ac.jp

This is an open-access article distributed under the terms of the Creative Commons Attribution Non-Commercial No Derivatives (by-nc-nd) License <http://creativecommons.org/licenses/by-nc-nd/4.0/>.

Copyright© 2025 by The Japanese Society for Pediatric Endocrinology

Introduction

Pediatric thyroid diseases encompass a wide spectrum of conditions and pose a significant concern within pediatric endocrine practice. Early diagnosis and intervention are vital to avert physical, cognitive, and psychosocial sequelae, including growth impairment, cognitive deficits, and behavioral alterations. Congenital hypothyroidism, in particular, represents a medical emergency, as delayed treatment may result in irreversible neurological damage. Comprehensive evaluation of thyroid function is critical for the accurate diagnosis and management of thyroid disorders in pediatric populations. Imaging techniques, when integrated with clinical assessment, provide indispensable diagnostic insight. Ultrasonography (US) serves as an efficient modality for evaluating thyroid morphology with precision. Scintigraphy using ^{123}I or ^{99m}Tc-pertechnetate facilitates a more detailed assessment of thyroid morphology, contributing to the understanding of underlying pathophysiological mechanisms and the extent of thyroid dysfunction. This review systematically examines the imaging findings associated with pediatric thyroid diseases.

Embryology and anatomy

The thyroid gland has a dual embryological origin, consisting of follicular and parafollicular cells. At approximately 24 d of gestation, follicular cells arise from the primitive pharyngeal floor situated between the first and second pharyngeal arches, while parafollicular cells develop from the lateral aspect of the fourth pharyngeal pouch. Follicular cells migrate to the anterior neck by 7 wk of gestation through the thyroglossal duct, a pathway extending from the cecal foramen at the base of the tongue to the orthotopic position in the anterior neck (**Fig. 1**). Ectopic thyroid tissue and thyroglossal cysts may form along this ductal route. While thyroid gland formation is complete by 8–10 wk of gestation, parafollicular cells integrate with the follicular cells, becoming dispersed throughout the thyroid gland. These parafollicular cells are responsible for the production of calcitonin, a hormone crucial for the regulation of calcium homeostasis.

The thyroid gland consists of the right and left lobes, connected by an isthmus, and is located in the anterior neck, extending from the level of the thyroid cartilage superiorly to the 5th–6th tracheal cartilage ring inferiorly (1). The pyramidal lobe, often extending cephalad from the isthmus, is a vestigial remanent of the thyroglossal duct. The thyroid gland is highly vascularized, receiving its blood supply from the superior thyroid artery, a branch of the external carotid artery, and the inferior thyroid artery, which originates from the subclavian artery.

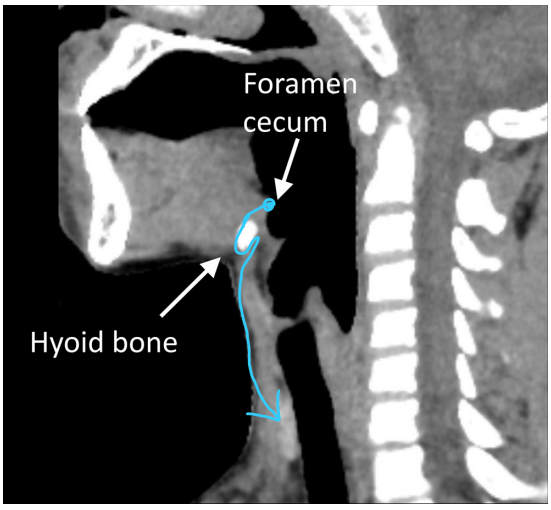

Fig. 1. Schema of the thyroid descending pathway (thyroglossal duct). A sagittal CT image of a healthy 12-yr-old boy is shown to illustrate this pathway. The thyroid bud originates at the foramen cecum, descends caudally, wraps from the caudal to the dorsal aspect of the hyoid primordium, and then descends anteriorly to the thyroid cartilage, ultimately reaching its final position.

Physiology

The thyroid hormones thyroxine (T4) and triiodothyronine (T3) play a critical role in regulating somatic growth, early brain development, thermoregulation, and energy metabolism. The production of thyroid hormones is tightly regulated through the hypothalamic-pituitary-thyroid axis, involving feedback mechanisms mediated by thyrotropin-releasing hormone (TRH), somatostatin, and thyroid-stimulating hormone (TSH). The thyroid hormones are composed of two tyrosine molecules and either three (T3) or four (T4) iodine (I) atoms. In the bloodstream, most circulating thyroid hormones are bound to serum proteins, with only trace amounts of free hormones exerting biological effects.

Thyroid hormones are synthesized from iodide (I^-) and thyroglobulin (TG) through a series of sequential steps (**Fig. 2**). TG is synthesized in follicular cells and subsequently secreted into the follicular lumen. Iodide (I^-) is actively transported into thyroid follicular cells via the sodium/iodide symporter (NIS), and is then transported into the follicular lumen by pendrin. In the follicular lumen, iodide is oxidized to reactive iodine (I^0), which is incorporated into the tyrosine residues of TG, forming monoiodotyrosine (MIT) and diiodotyrosine (DIT) through a process known as organification. Subsequently, MIT and DIT undergo coupling to form T3 and T4. The iodotyrosine derivatives (MIT, DIT, T3, and T4) and TG complexes are then internalized by follicular cells and released into the bloodstream following enzymatic cleavage by lysosomal proteases.

doi: 10.1297/cpe.2024-0082

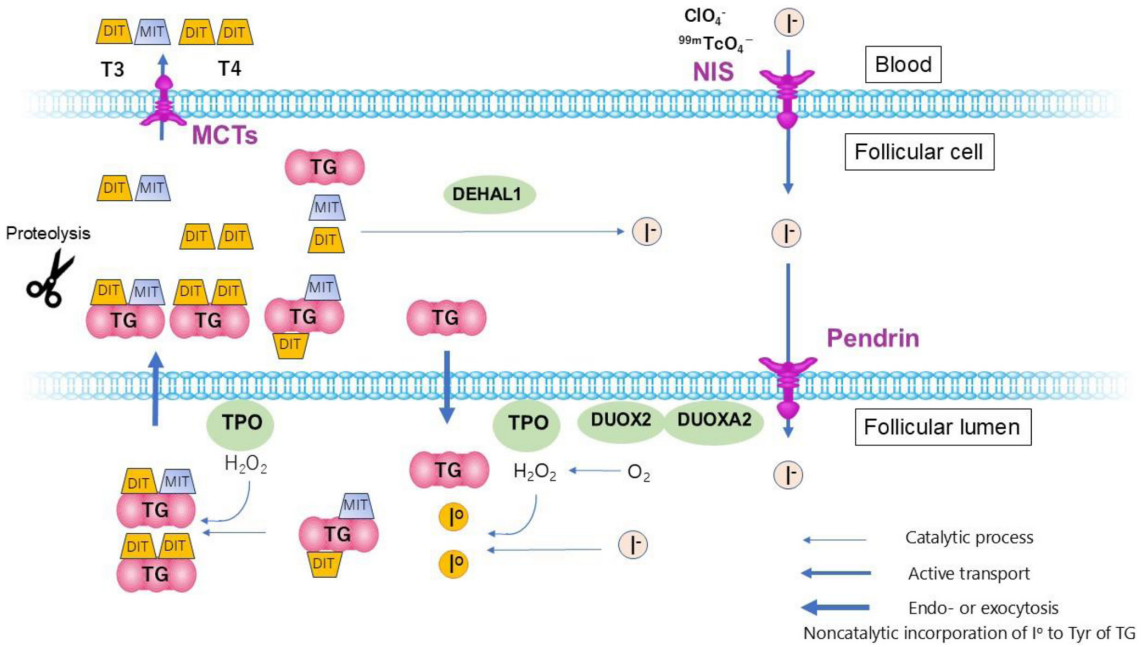

Fig. 2. Scheme of thyroid hormone synthesis. Thyroid hormone synthesis is a rate-limiting process regulated by several steps. TG is a polypeptide that serves as the template for thyroid hormone synthesis is produced in the endoplasmic reticulum of follicular cells and is transported into the follicular lumen via exocytosis. Iodide is actively transported into follicular cells through the NIS and then into the follicular lumen via pendrin. In the lumen, iodide is oxidized to reactive iodine by TPO, using hydrogen peroxide supplied by DUOX2 and its maturation factor DUOXA2. Reactive iodine is incorporated into the tyrosine residue of TG, a noncatalytic process. These oxidation and incorporation steps are termed "organification," resulting in the generation of MIT and DIT on TG. DIT-MIT and DIT-DIT are combined to form T3 and T4, a process catalyzed by TPO, known as "coupling." The TG-iodotyrosine (MIT, DIT, T3, and T4) complex is internalized into follicular cells via endocytosis and is then liberated into iodotyrosines through proteolysis. T3 and T4 are transported into the bloodstream via MCTs, which are essential for the cellular uptake of T3 and T4. MIT and DIT are deiodinated by DEHAL1. I^-, iodide; I^O, reactive iodine; I, iodine; tyr, tyrosine; H_2O_2, hydrogen peroxide; O_2, oxygen; NIS, Na+/I^- symporter; DUOXA2, dual oxidase 2 maturation factor; DUOX2, dual oxidase 2; TPO, thyroid peroxidase; MIT, monoiodotyrosine; DIT, diiodotyrosine; T3, triiodothyronine; T4, thyroxine; MCT, monocarboxylate transporter; DEHAL1, iodotyrosine dehalogenase 1.

T3 and T4 are released into the circulation, while MIT and DIT are deiodinated for iodine recycling.

Thyroid imaging

Ultrasound (US) is the primary imaging modality for evaluating pediatric thyroid diseases, providing valuable information regarding the echogenicity, size, vascularity, and characteristics of thyroid masses. The quality of the US examination depends significantly on the technical proficiency and experience of the examiner. Furthermore, US offers several advantages, including low cost, absence of radiation exposure, and no requirement for sedation. A high-frequency linear transducer, operating within the 10–18 MHz range, is typically employed. The quality of US images is influenced by hardware settings, such as total gain, dynamic range, maximum velocity, and other advanced image-processing techniques incorporated in modern equipment. These parameters are often tailored to the specific institution or the preferences of the examiner.

In normal thyroid parenchyma, the echotexture is homogeneous, and the echogenicity is slightly higher than that of the cervical muscles (**Fig. 3**) (2). Blood flow within the thyroid can be assessed using Doppler technology. In color Doppler imaging, red and blue colors represent flow toward and away from the probe, respectively, while other colors (e.g., yellow, orange, light blue, and green) indicate variations in flow speed or turbulence. However, the relationship between flow properties and the corresponding colors is influenced by the settings of the US equipment. Power Doppler imaging, which measures the amplitude of the Doppler signal generated by moving red blood cells, is more sensitive than color Doppler for detecting smaller velocities but does not provide information about flow direction.

Doppler US velocity measurements of the superior thyroid artery can quantitatively assess thyroid vascularity. The normal maximum velocity (V_{max}) is typically less than 25 cm/sec, with an average V_{max} of 21 cm/sec in children, lower than the V_{max} observed in adults (26 cm/sec in individuals aged 25–49 yr and 31 cm/sec in those aged >50 yr) (3). Shear wave elastography (SWE) is a novel technique that measures tissue stiffness and holds promise for distinguishing benign from malignant thyroid nodules (4–6). Thyroid volume can be

doi: 10.1297/cpe.2024-0082

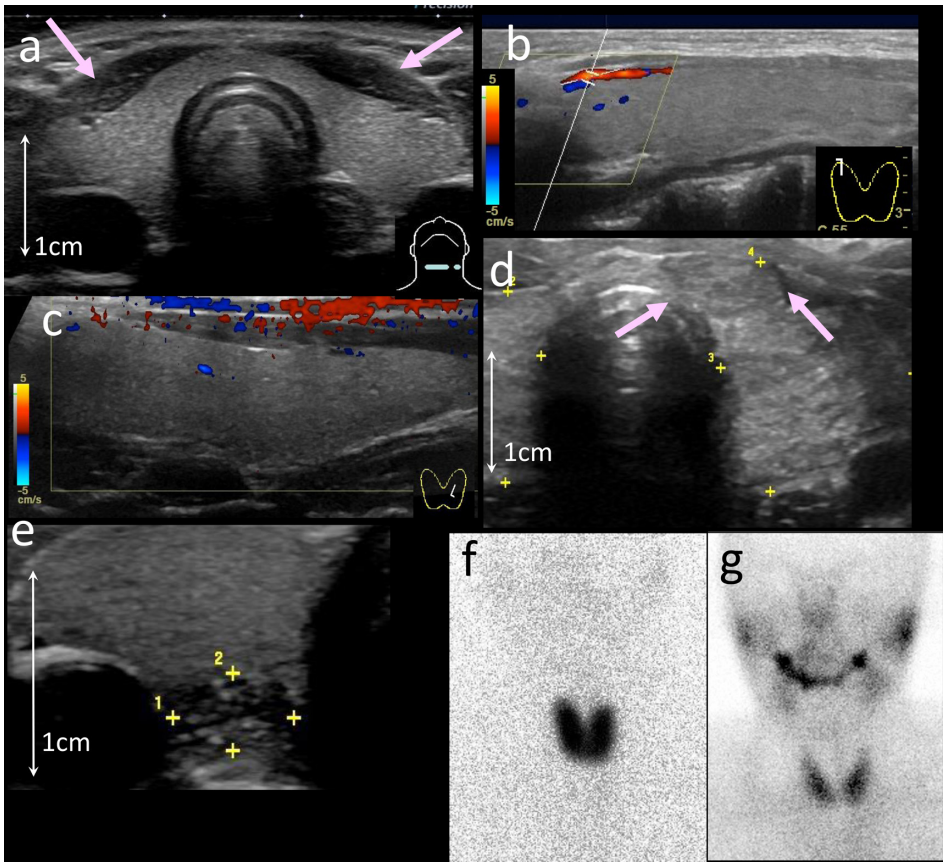

Fig. 3. Normal thyroid images in children: US (a–e) and scintigraphy (f, g). (a) The thyroid parenchyma appears homogeneously echogenic compared to the strap muscles (→) on ultrasound (US). (b) Flow velocity in the superior thyroid artery was measured at the upper pole of the thyroid gland. A maximum velocity (V_{max}) of < 25 cm/sec is considered normal in the pediatric population. (c) Color Doppler imaging reveals a normal pattern of intrathyroidal vasculature, depicted as small foci of flow signals scattered exclusively within the thyroid gland. (d) The pyramidal lobe is an embryological remnant of the thyroglossal duct, containing follicular cells, which extends upward from the isthmus (→). (e) Intrathyroidal ectopic thymus presents as a hypoechoic mass-like lesion with multiple internal linear and punctate bright foci, known as the "starry-sky" appearance on US. (f) A normal ^{123}I-scintigraphy delineates only the thyroid gland, whereas salivary glands are barely visible. (g) A normal ^{99m}Tc-pertechnetate scintigraphy reveals the thyroid gland and salivary glands.

calculated by measuring the anteroposterior, transverse, and vertical diameters, using the formula height × width × length × 0.523. Thyroid size may vary according to factors such as race and iodine intake; therefore, universally accepted reference values for normal thyroid size are lacking (7). However, reference values for thyroid size in Japanese children and adolescents have been reported (8). A common developmental variation of the thyroid gland is an intrathyroidal ectopic thymus, which may be misinterpreted as a pathological finding. However, US imaging can reveal the characteristic hypoechoic areas with multiple internal linear and punctate foci, known as a "starry-sky appearance" (**Fig. 3e**). Moreover, the ectopic intrathyroidal thymus is typically located in the dorsal aspect of the inferior thyroid gland.

Thyroid scintigraphy is performed following oral intake of Na^{123}I (half-life: 13 h) or intravenous administration of ^{99m}Tc-pertechnetate ($^{99m}TcO_4^-$; half-life: 6 h) (**Figs. 3f, g**). ^{123}I is transported into the follicular cell and is organized in the follicular lumen. ^{123}I-scintigraphy mirrors the iodine metabolism in the thyroid. The normal thyroid uptake of ^{123}I, also known as radioactive iodine uptake (RAIU), ranges from 10% to 35% at 24 h and 6% to 18% at 4 h post-administration (1). Additionally, the concurrent use of perchlorate (perchloride discharge test) in ^{123}I scintigraphy assists in diagnosing organification disorders, which are characterized by excessive iodide influx into the follicular cells. The perchlorate ion (ClO_4^-) competes with iodide (I^-) for transport into the follicular cells, leading to the leakage of iodide into the bloodstream. The washout rate of radioiodine, measured two hours after perchlorate administration, is typically less than 10% in healthy individuals. A washout rate exceeding 50% indicates complete organic failure, whereas a discharge rate of 20–50% suggests partial organic failure (1) (**Fig. 4**). The perchlorate test remains the only clinical tool used to confirm a provisional molecular diagnosis of an organification disorder. However, perchlorate is not approved for medical use in Japan, thus limiting its

doi: 10.1297/cpe.2024-0082

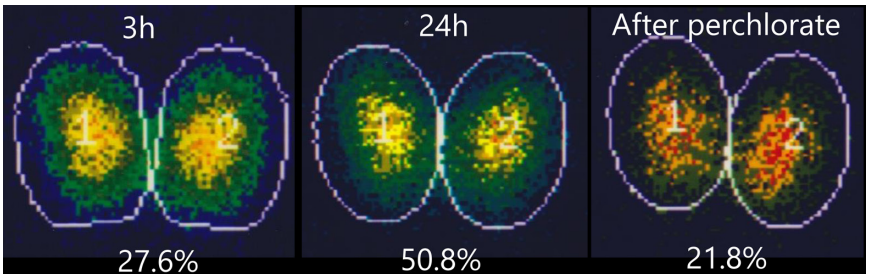

Fig. 4. Perchlorate discharge test. An 8-yr-old girl with an organization defect was diagnosed with hypothyroidism on neonatal screening. ^{123}I-scintigraphy shows a washout rate of > 50% after perchlorate administration (less than 10% in normal individuals), with 27.6% at 3 h and 50.8% at 24 h after ^{123}I administration, and 21.8% after administration of perchlorate.

Table 1. Comparison of thyroid scintigraphy nuclei (Na ^{123}I and ^{99m}Tc-pertechnetate ($^{99m}TcO_4^-$)

	Na ^{123}I	$^{99m}TcO_4^-$
Energy	Medium (159 keV)	Low (140 keV)
Effective dose	0.54 mSv/MBq	0.04 mSv/MBq
Cost	High	Low
Iodine restriction	May be necessary	Unnecessary
Physical half time	13 h	6 h
Image acquisition	3–6 h and 24 h	20–30 min
Reference value	6–18% (4 h), 10–35% (24 h)	0.3–3.0%
Uptake to salivary glands	±	++
Organification process evaluation	Possible	Impossible

※ On Na^{123}I scintigraphy, the uptake in the salivary glands was relatively low; thus, the glands were not clearly visible.

application in clinical practice.

A key disadvantage of radioiodine scintigraphy is the requirement for a one-week iodine restriction prior to the examination. $^{99m}TcO_4^-$ is trapped in the follicular cells but not in the follicular lumen, limiting its role in assessing thyroid function (9). Nonetheless, $^{99m}TcO_4^-$ is widely used because of its low cost, lack of special preparation requirements, high image quality with a short imaging time, and low radiation exposure (**Table 1**). Normal tracer uptake on $^{99m}TcO_4^-$ scintigraphy ranges from 0.3% to 3% (10).

Although computed tomography (CT) and magnetic resonance imaging (MRI) have limited roles in diagnosing endocrine thyroid diseases, these modalities are invaluable for identifying thyroid tumors and other space-occupying lesions. They provide precise information on the spatial relationships between thyroid lesions and adjacent structures. Furthermore, CT and MRI are essential for diagnosing central hypothyroidism caused by hypothalamic and pituitary lesions.

Overview of congenital hypothyroidism

Congenital hypothyroidism is the most prevalent congenital endocrine disorder, with an estimated incidence of 1/3000–4000 live births (11–13). Most affected neonates are identified through screening programs. However, the classical symptoms of congenital hypothyroidism, such as prolonged jaundice, hypotonia, umbilical hernia, and coarse facies, are rarely encountered in recent cases. Congenital hypothyroidism is classified into transient and permanent types. The majority of affected children have primary hypothyroidism, while central hypothyroidism remains uncommon. Thyroid dysgenesis accounts for approximately 80% of cases, whereas thyroid dyshormonogenesis for 15–20%. Notably, recent studies employing lower cutoff thresholds for TSH levels have observed an increase in the incidence of dyshormonogenesis (14). Imaging studies are essential for elucidating the underlying etiology of congenital hypothyroidism, alongside the initiation of hormone replacement therapy. The diagnostic accuracy is enhanced when US and scintigraphy are employed in tandem (15). These imaging modalities provide not only valuable insights into the pathogenic mechanisms but also prognostic information, and aid in the assessment of treatment efficacy.

Transient congenital hypothyroidism

Transient congenital hypothyroidism is characterized by thyroid hypofunction that does not necessitate long-term treatment. In the United States, levothyroxine therapy is discontinued after the age of 3 yr in approximately one-third of children diagnosed with congenital hypothyroidism through newborn screening

doi: 10.1297/cpe.2024-0082

(16). This group of disorders arises from *in utero* exposure to TSH receptor-blocking IgG antibodies (TSBAb), maternal use of anti-thyroid drugs transferred across the placenta, maternal iodine deficiency, or, paradoxically, excessive maternal iodine intake. Additionally, transient congenital hypothyroidism may result from various pathogenic variants of *DUOX2* (17) or functional immaturity of the thyroid gland.

US typically reveals a normal thyroid or a mild goiter, with large goiters being rare (**Fig. 5**). Further imaging is generally not necessary. However, scintigraphy may be useful in the differential diagnosis. Radiotracer uptake is decreased in TSBAb-induced thyroid dysfunction and increased in cases of maternal iodine deficiency or anti-thyroid drug ingestion (15). When scintigraphy is indicated, it should be performed within five days of initiating hormone therapy.

Thyroid dysgenesis

Thyroid dysgenesis refers to the abnormal organogenesis of the thyroid gland, typically identified as an isolated anomaly. Most cases of thyroid dysgenesis are polygenic disorders, resulting from mutations in multiple thyroid-related genes and *in utero* environmental factors (18). Recent studies have shed light on the genetic factors underlying thyroid dysgenesis. A SNP at 2q33.3, designated rs9789446, has been shown to increase the risk for thyroid aplasia and ectopia, but not for hypoplasia (19). Moreover, a recent association has been reported between variants in a noncoding TTTG microsatellite on 15q26.1 and non-goitrous congenital hypothyroidism (20). Only a small proportion of thyroid dysgenesis cases (1–3%) are monogenic disorders that manifest either as isolated thyroid malformations or as part of multi-system disorders. The former includes mutations in *TSHR* and *PAX8*, while the latter those in *NKX2-1* and *FOXE1*.

Thyroid dysgenesis is classified into four categories: agenesis, hemiagenesis, ectopia, and hypoplasia. Most cases of hemiagenesis and hypoplasia can be diagnosed using US. However, ectopic thyroid glands are often challenging to visualize with US. In cases where the thyroid gland is not visible in its normal (orthotopic)

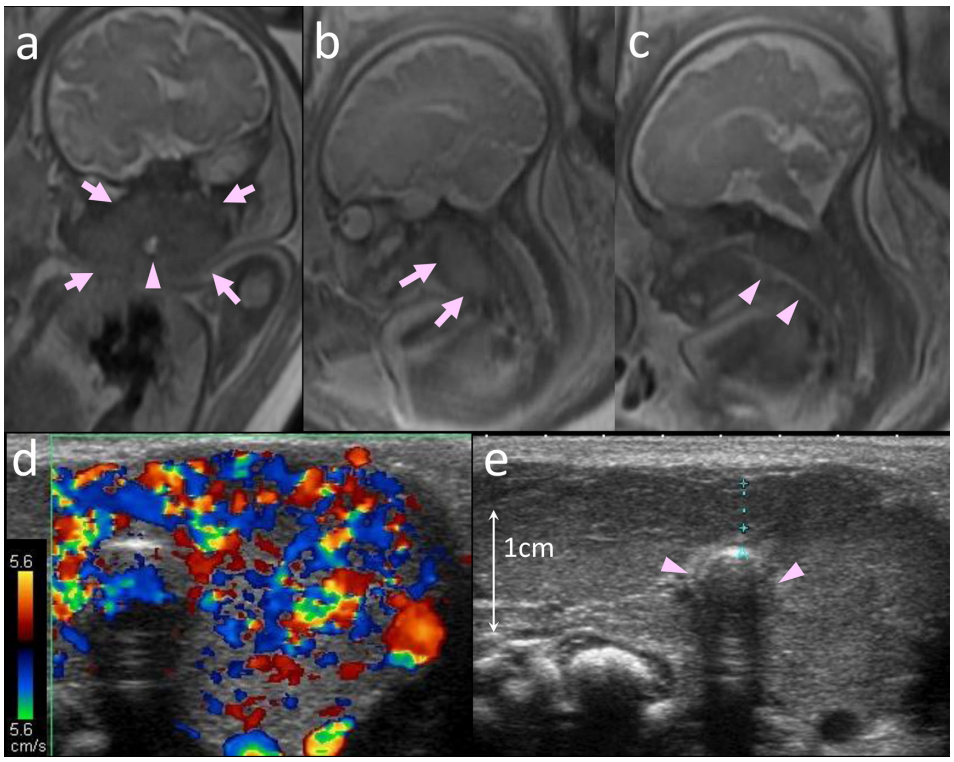

Fig. 5. Transient congenital hypothyroidism. The neonate presented with a severe prenatal goiter and transient hypothyroidism. Fetal magnetic resonance imaging (MRI) was performed with coronal (a), paramedian sagittal (b), and median sagittal (c) views. MRI shows massive thyroid enlargement (arrows in a, b) and constriction of the tracheal lumen (arrowheads in a, c). The enlarged thyroid gland appears as a bilateral, symmetrical cervical mass with intermediate signal intensity on the coronal image (a). Its extension from the nasopharynx to the thoracic inlet is observed on the paramedian sagittal image (b). The trachea, filled with fetal fluid, appears to have high intensity. The coronal image depicts the trachea as an oblong structure (a). The median sagittal image shows diffuse tracheal narrowing (c). Postnatal color Doppler and 2D ultrasound (US) images are shown in panels (d) and (e). The Doppler image demonstrates thyroid enlargement with an increased vascular signal, represented by large foci of red and blue colors, along with a mosaic pattern of mixed colors indicating plethora and turbulent flow, respectively. The US image clearly delineates the tracheal compression and thyroid enlargement (arrowheads).

doi: 10.1297/cpe.2024-0082

position, thyroid agenesis or an ectopic thyroid should be suspected. While the diagnosis of absent thyroid tissue is straightforward, some diagnostic challenges remain. For instance, US may reveal small, triangular, echogenic tissue lateral to the trachea during thyroid agenesis, which can be misinterpreted as thyroid hypoplasia (**Fig. 6**). This abnormal tissue represents remnants of branchial structures that failed to develop into the thyroid gland and often regress spontaneously with age (21). Additionally, a reduced distance between the right and left common carotid arteries may help confirm the absence of the thyroid gland in the orthotopic position.

Ectopic thyroid glands are more common than thyroid agenesis. Ectopic thyroid tissue can be located anywhere along the thyroglossal duct, laterally in the neck, or even at distant sites (22). The ectopic thyroid tissue most frequently occurs in the tongue base, where it may cause dysphagia and airway obstruction (**Fig. 7**) (23). Lingual ectopic thyroid glands typically appear round but may occasionally be dumbbell-shaped or hourglass-shaped, suggesting incomplete migration of the dorsal segment. Rare forms of ectopic thyroid tissue include sublingual, prelaryngeal, mediastinal, and intratracheal lesions. The diagnostic sensitivity of US in detecting ectopic thyroid varies between 21% and 78%, likely influenced by technical factors and equipment variations (15, 24). When US fails to confirm the presence of ectopic thyroid tissue, scintigraphy may be indicated, with a wide collimation that includes the tongue base and upper mediastinum. Noncontrast CT can also be useful in delineating the high attenuation of iodine in ectopic thyroid tissue. A thyroglossal duct cyst can occur at any point along the thyroglossal duct (**Fig. 8**). As noted, accurately diagnosing ectopic thyroid tissue using US alone is often difficult. Surgical intervention should be considered for symptomatic lesions, and the presence of an orthotopic thyroid gland should be confirmed with US. In cases where the orthotopic thyroid gland is absent, scintigraphy can confirm the presence of iodine uptake corresponding to the cyst, as small amounts of thyroid tissue within the thyroglossal cyst may retain partial thyroid function.

Thyroid hemiagenesis most commonly occurs on the left side. Affected children often present with a euthyroid state, owing to compensatory hypertrophy of the remaining thyroid gland. This hypertrophic gland may present as a palpable mass, drawing clinical attention. US typically shows a normal thyroid on one side and the absence of a thyroid on the other. The diagnosis of thyroid hypoplasia is based on volume calculations, with the tracheal index (calculated as the ratio of thyroid width to tracheal width, with values < 1.7 indicating hypoplasia). Hypoplastic thyroid glands tend to appear round, in contrast to the normal oblong shape of the thyroid.

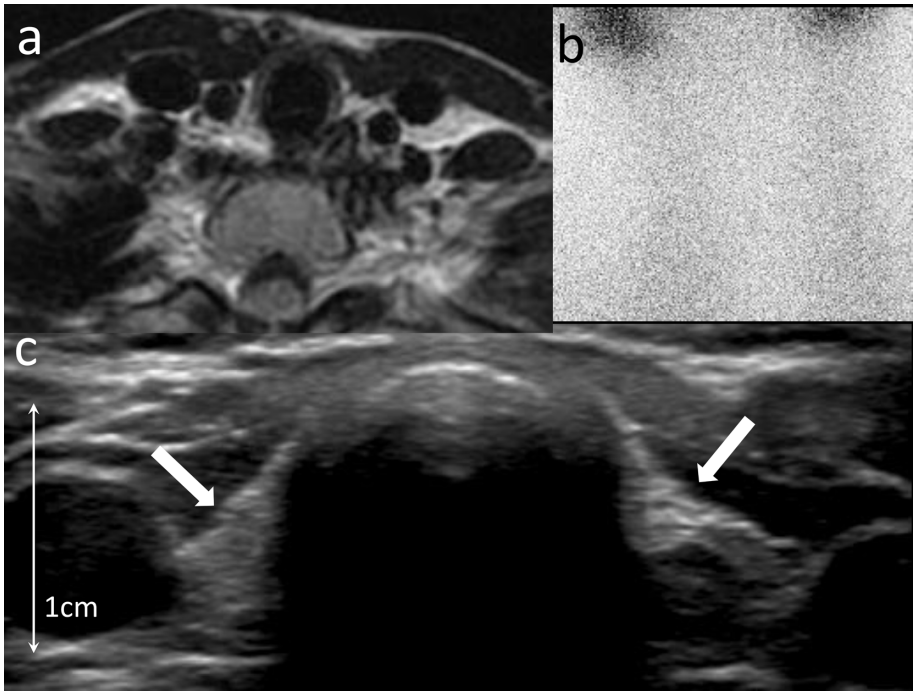

Fig. 6. Thyroid agenesis. A neonate was diagnosed with thyroid agenesis through neonatal screening. (a, b) MRI does not reveal an orthotopic thyroid gland. $^{99m}TcO4^-$ scintigraphy demonstrates normal salivary uptake but no orthotopic thyroid uptake. (c) Ultrasound (US) shows bilateral, symmetrical, small, triangular echogenic tissues in the juxtatracheal regions (arrows), which are presumed to be remnants of branchial tissues that failed to develop into the thyroid. This finding is occasionally observed in infants with thyroid agenesis and should not be mistaken for hypoplastic thyroid glands.

doi: 10.1297/cpe.2024-0082

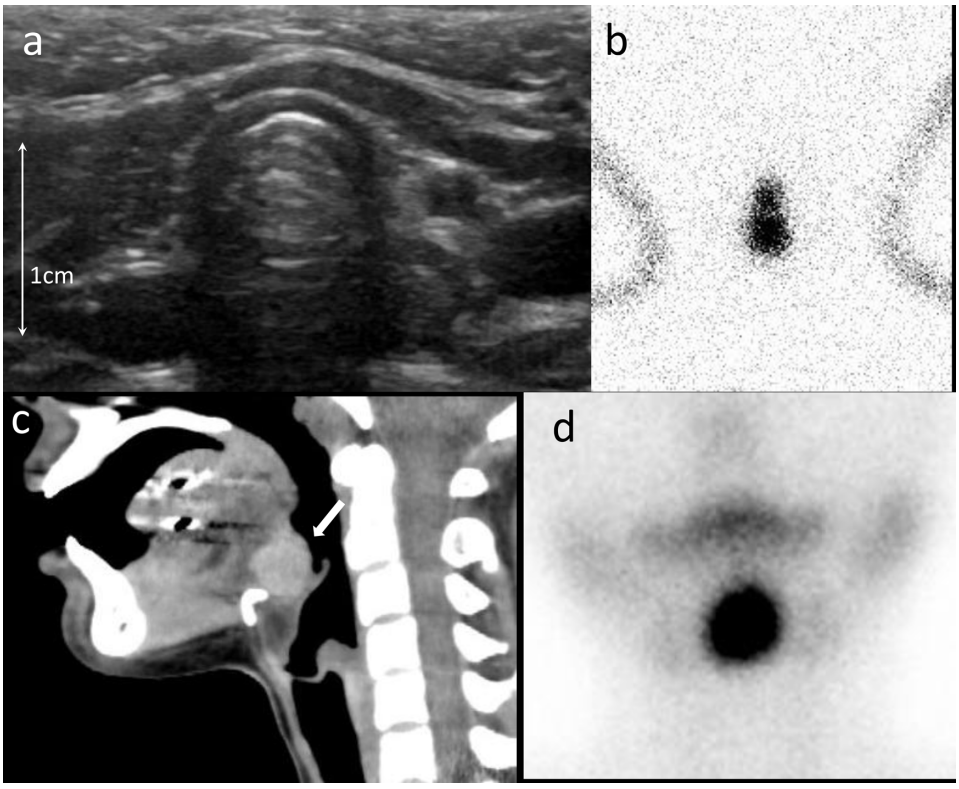

Fig. 7. Two cases of ectopic thyroid. A neonate with ectopic thyroid was diagnosed during screening. (a, b) Ultrasound (US) does not reveal an orthotopic thyroid. ^{123}I scintigraphy demonstrates dumbbell-shaped ectopic thyroid tissue at the tongue base. A child with thyroid ectopy at the base of the tongue presented with "throat discomfort." (c, d) Non-contrast CT shows a hyperdense ectopic thyroid at the tongue base (arrow), and $^{99m}TcO_4^-$ scintigraphy showing round tracer uptake.

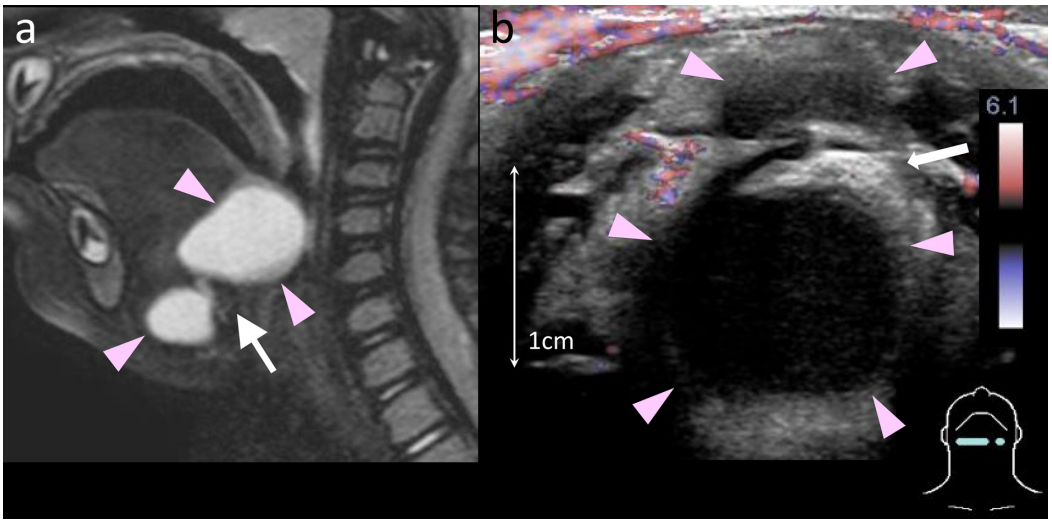

Fig. 8. Bilobed thyroglossal duct cyst. A 7-yr-old boy presented with swallowing difficulty. (a) Sagittal T2-weighted imaging shows an hourglass-shaped cystic lesion (arrowheads) but does not clearly delineate the hyoid bone (→). (b) In contrast, ultrasound (US) clearly shows the relationship between the hourglass-shaped cyst (arrowheads) and the hyoid bone (→).

Thyroid dyshormonogenesis

Thyroid dyshormonogenesis comprises a heterogeneous group of inborn errors in thyroid hormone synthesis resulting from single-gene defects, such as those in *SLC5A5*, *TG*, *SLC26A4*, *TPO*, *DUOX2*, *DUOXA2*, and *DEHAL1*. While these disorders are inherited as an autosomal recessive trait, heterozygous variants may

doi: 10.1297/cpe.2024-0082

increase susceptibility to congenital hypothyroidism (25). Dyshormonogenesis typically presents as thyroid enlargement; however, goitrous changes may remain unrecognized during infancy or develop later in childhood. Radiotracer uptake is increased in all types of dyshormonogenesis, except for NIS deficiency (iodine concentration disorders). On US, the internal texture of the thyroid is generally homogeneous, and the blood flow signal is often enhanced. It has been reported that the echotexture in dyshormonogenesis tends to be more uniform than that observed in Graves' disease, even when thyroid enlargement and increased blood flow signals are similar between the two conditions (26). A few studies have suggested that measurements of the "vascularity index" (the ratio of color pixels to the total pixels within a selected region) correlate well with the degree of thyroid hypofunction (27).

NIS deficiency that is caused by mutations in *SLC5A5* gene can be diagnosed through thyroid scintigraphy. The *SLC5A5* gene encodes the Na^+/I^- symporter, which is expressed not only in the thyroid gland but also in the salivary glands. Thyroid scintigraphy in NIS deficiency typically reveals substantially decreased uptake, often almost no uptake, in both the thyroid and salivary glands (**Fig. 9)**.

Pendred syndrome is characterized by congenital hypothyroidism and sensorineural hearing loss, both of which are caused by mutations in the *SLC26A4* gene, which encodes pendrin. Pendrin deficiency impairs iodide (I^-) availability for organification, leading to a partial organification defect. Hypothyroidism in Pendred syndrome is usually mild, and many children remain undiagnosed until adolescence (17). Auditory morbidity results from inner ear anomalies, which can be delineated using CT and MRI (**Fig. 10**) (27). Pendred syndrome accounts for 4–10% of congenital hearing impairments.

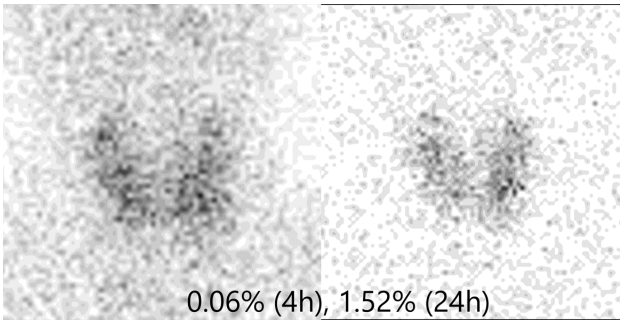

Fig. 9. Dyshormonogenesis due to NIS dysfunction. A 10-yr-old girl with NIS dysfunction diagnosed on neonatal screening (TSH, 807 μIU/mL; fT4, 0.1 ng/dL; fT3, 3.9 pg/mL). ^{123}I-scintigraphy shows a trace amount of tracer uptake in the thyroid gland.

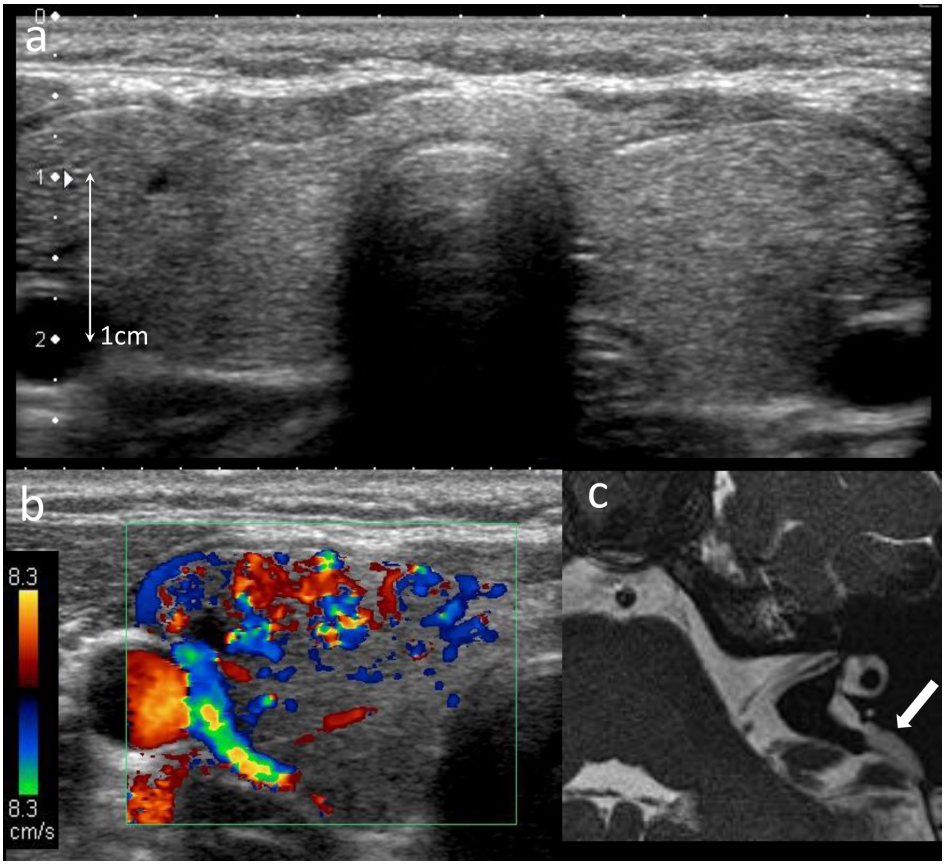

Fig. 10. Pendred syndrome. A 13-yr-old girl with goiter and bilateral hearing loss was diagnosed at 4 yr of age. (a, b) US showing thyroid gland enlargement associated with increased vascularity. (c) Heavy axial T2-weighted image showing enlargement of the vesicular aqueduct (arrow). The cochlea appeared normal (data not shown).

doi: 10.1297/cpe.2024-0082

Organizational disorders are the most common type of thyroid dyshormonogenesis. These inborn errors are caused by defects in the TPO/DUOX2/DUOXA2 complex, which is essential for I^- oxidation. The perchlorate test reveals high washout rates of ^{123}I in these cases. Furthermore, US typically shows thyroid enlargement with hypervascularity (**Fig. 11**). TPO deficiency is frequent in Caucasians and manifests as severe goitrous hypothyroidism. DUOX2 deficiency is more frequent in Asians, where it typically presents as mild hypothyroidism that often improves with age. DUOXA2 deficiency is a rare cause of congenital hypothyroidism (28).

TG deficiency presents as goitrous hypothyroidism, which is usually detected during newborn screening and demonstrates markedly increased radiotracer uptake (29). Low serum TG levels are a diagnostic laboratory finding in this disorder. The final step of thyroid hormone organization is thought to be impaired in TG deficiency, although the perchlorate test is normal in this condition. Iodothyrosine deiodinase, encoded by the *DEHAL1* gene (formerly called *IYD*), is involved in the recycling of I^-. Its deficiency results in increased urinary levels of MIT and DIT.

Congenital central hypothyroidism

Congenital central hypothyroidism encompasses a range of disorders, including pituitary stalk interruption syndrome, septo-optic dysplasia, and hypothalamic or pituitary gland compression due to space-occupying lesions (**Fig. 12**). This condition may be missed during TSH-based newborn screening. Most cases of central hypothyroidism are associated with deficiencies in other pituitary hormones, leading to clinical manifestations such as hypoglycemia and micropenis or undescended testes, which often prompt medical evaluation. Isolated TSH deficiency is linked to genetic defects in the TSH biosynthetic pathway, including mutations in *TSHB*, *TRHR*, and *IGSF1* (30).

Congenital hyperthyroidism

Most cases of congenital hyperthyroidism result from the transplacental transfer of stimulating TSH receptor antibodies (TSAb) from mothers with Graves' disease. Preterm delivery and non-immune fetal hydrops are commonly observed. Prenatal US often reveals a

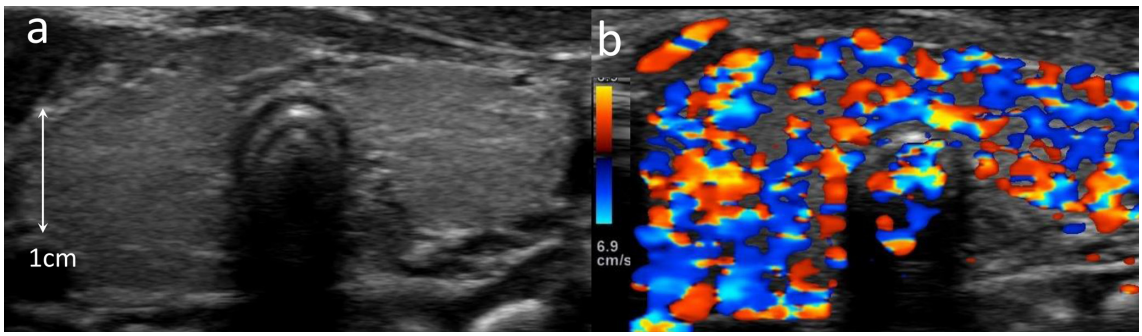

Fig. 11. DUOX2 abnormalities. A neonate with dyshormonogenesis due to biallelic pathogenic variants in the *DUOX2* gene, presenting with jaundice (TSH, 87 μIU/mL; fT4, 0.79 ng/dL; fT3, 3.48 pg/mL). (a, b) Ultrasound (US) shows thyroid enlargement with a markedly increased flow signal.

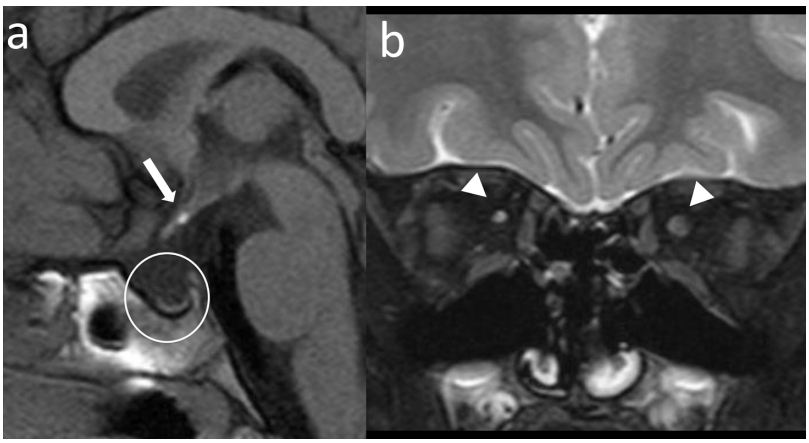

Fig. 12. Septo-optic dysplasia. A 6-yr-old child, presenting with refractory hypoglycemia and hypothyroidism. (a, b) MRI shows the absence of the pituitary gland (circle) with an interrupted pituitary stalk and an ectopic posterior lobe (arrow). Hypoplastic optic nerves (arrowheads).

doi: 10.1297/cpe.2024-0082

fetal goiter and growth restriction. Affected neonates typically present with tachycardia, accelerated skeletal maturation, and, in some cases, craniosynostosis (31, 32). Since the half-life of TSAb is approximately 12 d, hyperthyroidism generally resolves shortly after birth. Persistent hyperthyroidism lasting more than 2–3 mo warrants consideration of other conditions, such as activating mutations in the *TSHR* gene (33) and McCune–Albright syndrome (34). McCune–Albright syndrome is characterized by a triad of polyostotic fibrous dysplasia, café-au-lait spots, and precocious puberty. It is caused by somatic mutations in the *GNAS* gene, leading to the constitutive activation of G protein-coupled hormone receptors, including TSH and gonadotropin receptors. Hyperthyroidism is the second most common endocrine abnormality associated with McCune–Albright syndrome. The severity of thyroid hyperfunction varies across studies. In severe cases of thyrotoxicosis, radioablation may be necessary. Affected children may develop micronodular goiters, which are characterized by progressively enlarging nodules with heterogeneous echotexture and increased vascular flow signals on US (**Fig. 13**) (35).

Acquired thyroid disease in older children and adolescents

Mild cases of congenital hypothyroidism may attract medical attention during school age or adolescence, and hypothyroidism secondary to iodine deficiency/excess, anti-thyroid medications, or radioisotope ablation therapy is rarely observed in older children and adolescents. Central hypothyroidism in this age group is typically attributed to hypothalamic-pituitary tumors or tumor-like lesions. Autoimmune thyroiditis is a common condition in older children and adolescents, with Hashimoto's thyroiditis being more prevalent than Graves' disease. Subacute thyroiditis is a relatively rare condition in this age group.

The clinical symptoms of acquired thyroid diseases are similar to those seen in adults; however, certain issues are unique to children. These include a decelerated growth rate and delayed puberty in hypothyroidism, and an accelerated growth rate in hyperthyroidism. Unusual behavior and poor academic performance are also common presenting problems. In this section, we briefly discuss the imaging findings of autoimmune and non-autoimmune thyroiditis.

Hashimoto's thyroiditis is the most common cause of acquired hypothyroidism in children. This disorder occurs in 1–2% of school-aged children, and 6–8% of adolescents have positive thyroid autoantibodies (36). Early manifestations include compensated euthyroidism or hyperthyroidism with elevated TSH levels, subclinical hypothyroidism, and goiter. Early imaging findings include increased radiotracer uptake on scintigraphy and thyroid enlargement with increased blood flow signals on US (**Figs. 14a, b**) (37). Differential diagnosis between Hashimoto's thyroiditis with thyrotoxicosis and Graves' disease can be challenging based on clinical and imaging findings alone. However, a few imaging characteristics can aid in differentiation. Hashimoto's thyroiditis

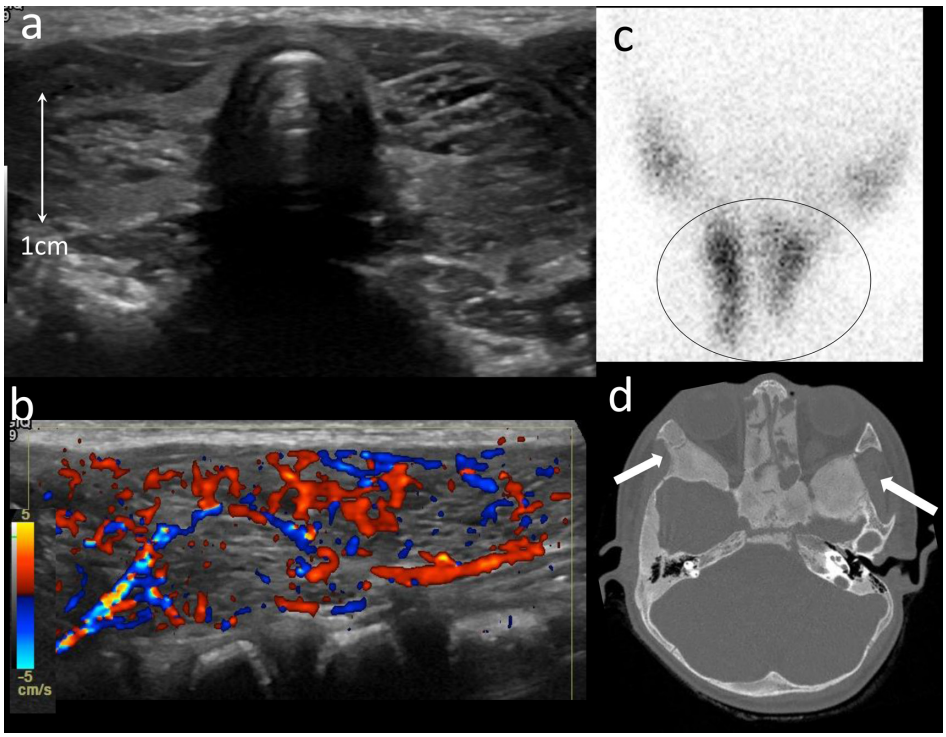

Fig. 13. McCune-Albright syndrome. A 1-yr-old girl with McCune-Albright syndrome. (a, b) US shows heterogeneous echogenicity with increased vascular signals. (c) $^{99m}TcO_4^-$ scintigraphy showing inhomogeneous tracer uptake. (d) Polyostotic fibrous dysplasia of the craniofacial bones is found on CT.

doi: 10.1297/cpe.2024-0082

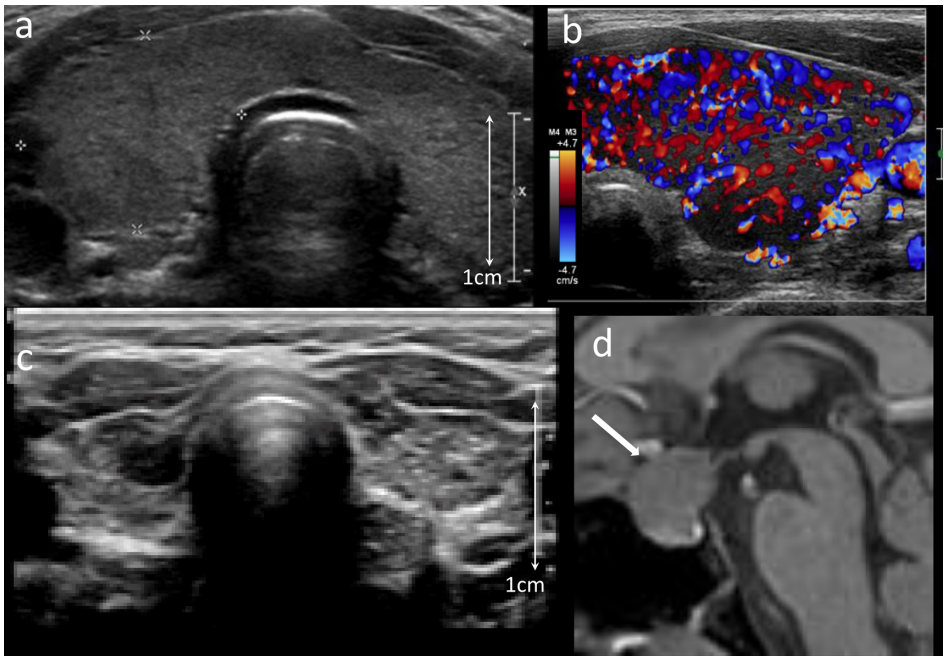

Fig. 14. Two cases with autoimmune thyroiditis. A 9-yr-old girl with Hashimoto's thyroiditis, presenting with fatigability and loss of concentration (fT4, 0.56 ng/dL; fT3, 4.0 pg/mL; TSH, 61.3 μIU/mL; positive anti-TPO antibody, (> 600 IU/mlL), and positive antithyroglobulin antibodies (308 IU/mL)). (a, b) Ultrasound (US) shows heterogeneous internal echogenicity with surface irregularities and markedly increased vascularity, a constellation of findings typical for childhood Hashimoto's thyroiditis.An 11-yr-old girl with atrophic thyroiditis, presenting with abrupt growth arrest and fatigability (fT3, 0.79 pg/mL; fT4, 0.11 ng/dL; TSH, 1,835 μIU/mL; elevated TSB-Ab, (39.5%)). (c, d) US shows atrophy of the thyroid gland with heterogeneously decreased parenchymal echogenicity and decreased vascularity (not shown). MRI reveals pituitary enlargement secondary to TSH overproduction (arrow).

typically presents as multinodular hypoechogenicity or heterogeneous echogenicity, whereas Graves' disease tends to show less heterogeneous echogenicity. The average peak systolic velocity of the superior thyroid artery has been reported to be 51 cm/sec in Hashimoto's thyroiditis, compared to 88 cm/sec in Graves' disease (3). RAIU on ^{123}I scintigraphy is lower in Hashimoto's thyroiditis than in Graves' disease. Furthermore, the T3 suppression test, although rarely used, significantly decreases the RAIU in Hashimoto's thyroiditis. The final diagnosis depends on the careful integration of endocrine, serological, and imaging findings. As the disease progresses, the severity of hypothyroidism increases, and late imaging findings include thyroid atrophy and reduced radiotracer uptake.

Atrophic thyroiditis (AT; delete) is a subtype of autoimmune thyroiditis in which hypothyroidism is more severe than in typical Hashimoto's thyroiditis, often accompanied by secondary pituitary enlargement. Thyroid atrophy in this form progresses rapidly (**Figs. 14c, d**). Affected individuals frequently seek medical attention due to decelerated physical growth.

Graves' disease occurs in approximately 1 in 5,000 children, with a higher incidence in females (36). Diagnosis is primarily based on clinical and laboratory findings; however, imaging studies can help distinguish Graves' disease from destructive thyroiditis, such as subacute thyroiditis. Radiotracer uptake is markedly increased in Graves' disease but reduced in destructive thyroiditis. RAIU typically rises to approximately 50% at 4 h and 75% at 24 h (normal: 5–12% at 4 h and 10–30% at 24 h) (24). US typically shows a diffuse goiter with heterogeneously decreased internal echogenicity and markedly increased blood flow signals, often described as a hypervascular "thyroid inferno" (**Fig. 15**) (31).

Subacute thyroiditis can be classified into subacute lymphocytic thyroiditis and subacute granulomatous thyroiditis (de Quervain's thyroiditis). The former is often autoimmune or drug-induced, such as by interferon or amiodarone, while the latter is typically triggered by viral infections. Both types are pathologically destructive forms of thyroiditis. Scintigraphy in these cases reveals markedly decreased radiotracer uptake (**Fig. 16**).

Space-occupying lesions in the thyroid gland

Branchial anomalies can present as thyroid or juxtathyroidal masses. Pyriform sinus fistulas commonly lead to acute suppurative thyroiditis in young children, which manifests as an intrathyroidal abscess with adjacent soft tissue edema on US and other sectional imaging modalities. Fistulous remnants of the third or fourth branchial cleft are frequently observed on the left side (38). Barium swallow imaging is utilized to identify the sinus tract extending from the hypopharynx to the

doi: 10.1297/cpe.2024-0082

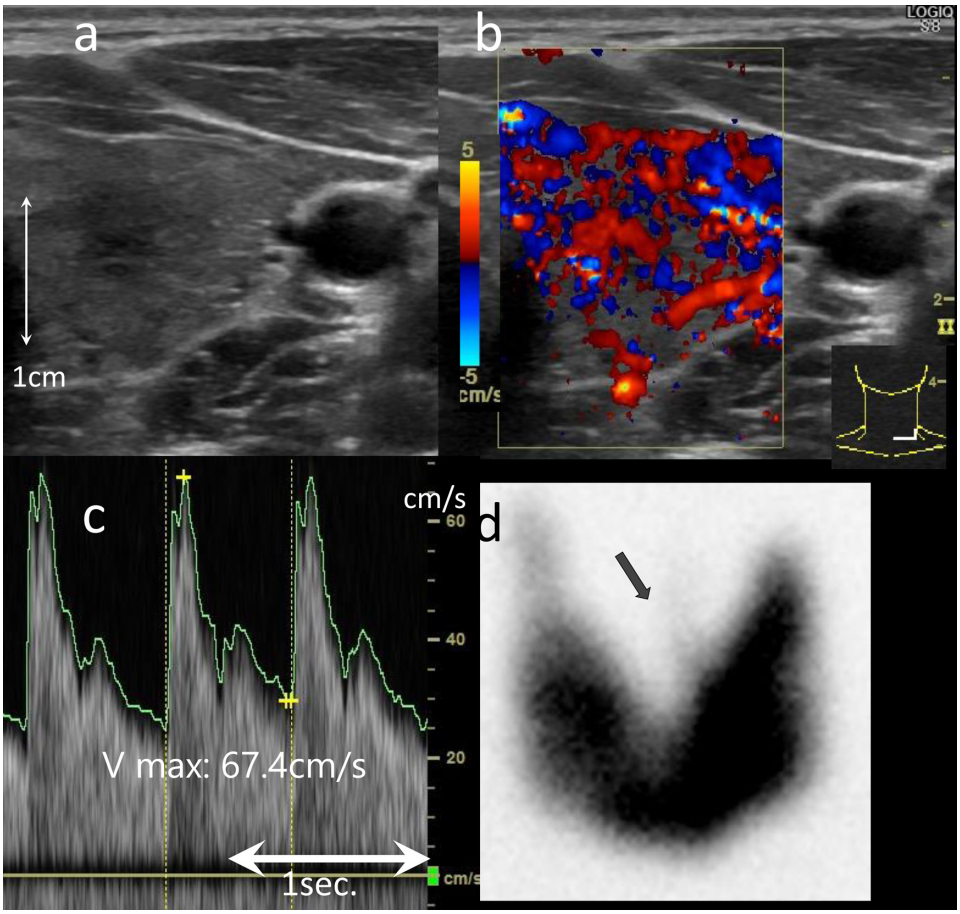

Fig. 15. Graves' disease. A 10-yr-old boy with Graves' disease presented with fatigue and excessive sweating (fT4, 5.0 ng/dL; fT3, 14.5 pg/mL; TSH, < 0.01 μIU/mL). (a–c) US shows thyroid enlargement with heterogeneous echogenicity and increased vascularity (thyroid inferno). The maximum velocity (V_{max}) of the superior thyroid artery is measured at 67.4 cm/sec (the average in the pediatric population is 21 cm/sec). (d) ^{123}I-scintigraphy shows diffusely increased tracer uptake. The pyramidal lobe is also visible (arrows).

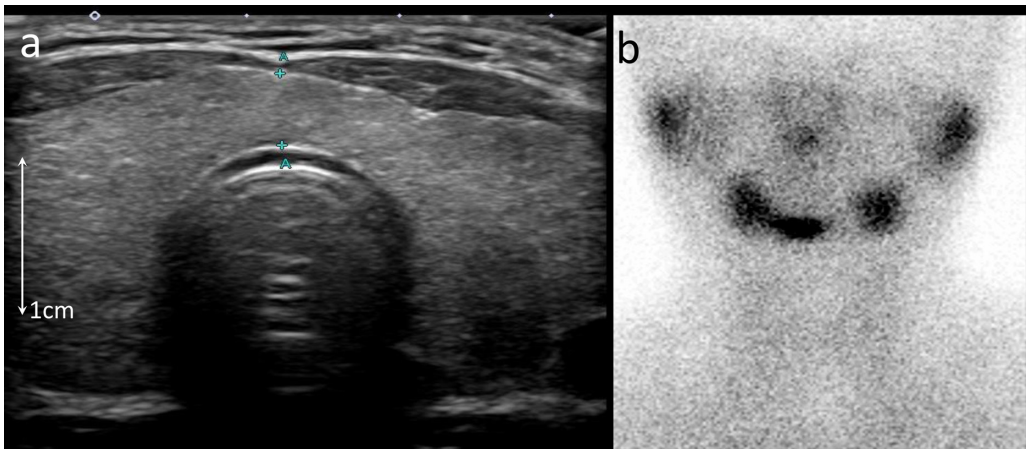

Fig. 16. Drug-induced thyroiditis. An adolescent girl who received treprostinil for pulmonary hypertension developed severe diarrhea (fT3, 7.1 pg/mL; fT4, 3.3 ng/dL; TSH, 0.07 μIU/mL). (a) Ultrasound (US) shows diffuse thyroid gland enlargement with slightly heterogeneous echogenicity. (b) $^{99m}TcO_4^-$ scintigraphy shows decreased uptake (tracer uptake: 0.36%, reference value: 0.4–2.5%), which is compatible with destructive thyroiditis.

thyroid gland; however, this procedure is not always successful (**Fig. 17**).

Pediatric endocrinologists often collaborate in the multidisciplinary management of children with thyroid tumors. Pediatric thyroid tumors are most commonly diagnosed in children over the age of 10 yr.

doi: 10.1297/cpe.2024-0082

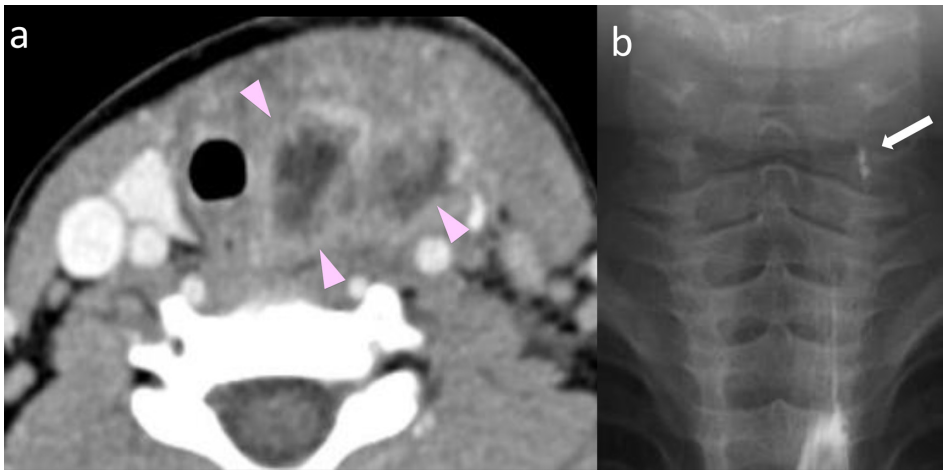

Fig. 17. Acute thyroiditis associated with pyriform sinus fistula. A 3-yr-old boy with anterior neck pain and fever. (a) Contrast-enhanced CT shows left thyroid swelling with internal liquefied foci suggestive of an abscess (arrowheads). (b) Barium swallowing examination reveals a pyriform sinus fistula (arrow).

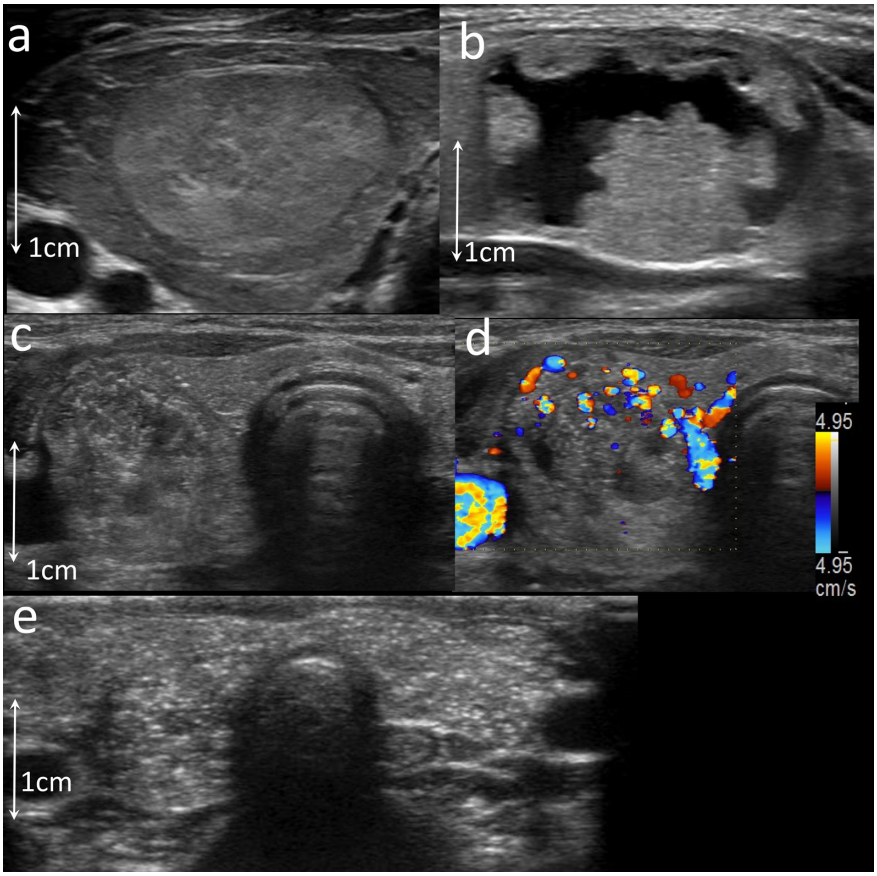

Fig. 18. Benign and malignant lesions. (a) Follicular adenoma found in a 12-yr-old girl is depicted as a well-margined mass with homogeneously hyperechoic echotexture, associated with a thin peripheral halo. (b) Adenomatous hyperplasia or adenomatous nodule in a 13-yr-old boy manifests as an admixture of solid and cystic components, but the lesion is well-defined. (c, d) Papillary carcinoma in a 10-yr-old girl is delineated as having heterogeneous internal echotexture with multiple calcifications (depicted as "twinkling artifacts" or artifacts related to inherent noise within the color-Doppler scanner) and an irregular vascular signal. (d) Diffuse sclerosing variant of papillary carcinoma in an 11-yr-old girl is depicted as extensive hyperechoic speckles that reflect diffusely scattered microcalcifications, referred to as the "snowstorm appearance."

doi: 10.1297/cpe.2024-0082

While a comprehensive discussion of oncological issues is beyond the scope of this study, it is important to note a few distinctive characteristics of thyroid tumors in children. Pediatric thyroid tumors are more likely to be malignant, with 22–26% of thyroid nodules in children being malignant, compared to only 5–10% in adults (39). As in adults, most malignant tumors in children are well-differentiated. Papillary carcinoma accounts for 85% of cases in affected children. Less common variants include follicular carcinoma, medullary carcinoma, diffuse sclerosing variants of papillary carcinoma, and, rarely, malignant lymphoma. Medullary carcinoma, which originates from parafollicular cells, is often associated with familial cancer syndromes, such as multiple endocrine neoplasia type 2. Unlike other malignant tumors, medullary carcinoma is more prevalent in infancy (40, 41). ^{123}I-scintigraphy scintigraphy plays a role in tumor differentiation. "Hot nodules" typically indicate benign tumors. However, malignant tumors that maintain NIS expression may present as hot lesions. The high degree of differentiation in pediatric thyroid cancer contributes to its generally better prognosis compared to adult thyroid cancer (42). It has been reported that 30% of "hot nodules" in children are malignant, a much higher percentage than the 3% observed in adults (43).

A high index of suspicion for malignant thyroid tumors is raised based on US findings, including irregular margins, hypervascularity with irregular internal flow signals, and "marked hypoechoic" nodules (hypoechoic compared to the overlying strap muscle), as well as extrathyroidal extension and adjacent lymphadenopathy (**Fig. 18**) (44). The diffuse sclerosing variant of papillary carcinoma presents with distinct pathological and imaging features. This tumor is characterized by diffuse lymphocytic infiltration with psammoma bodies and fibrosis, with the parenchyma of the unilateral thyroid gland potentially being completely replaced by tumor cells. US typically reveals diffuse thyroid enlargement with a speckled pattern of microcalcifications, often referred to as a "snowstorm appearance" (**Fig. 18d**) (45). The intratumoral calcifications may resemble echogenic spots seen in intrathyroidal ectopic thymic tissues, exhibiting the 'starry-sky appearance.' However, the calcifications in papillary carcinoma are generally brighter and smaller than those seen in ectopic thymic tissue (46).

Conflict of interests: The authors have nothing to declare.

Acknowledgement

We are grateful to Drs. Koji Muroya and Keisuke Nagasaki for teaching the first author (YT) the endocrinological perspective on thyroid diseases in children and for providing key images for this work. We also thank Dr. Gen. Nishimura, Dr. Tatsuo Kono, Dr. Tomohiro Ishi, and Dr. Kiyomi Abe for their assistance in completing this study.

References

1. Coley BD. Caffey's pediatric diagnostic imaging. 13th ed ed: Elsevier; 2019. 2 v. p.
2. Chang YW, Hong HS, Choi DL. Sonography of the pediatric thyroid: a pictorial essay. J Clin Ultrasound 2009;37: 149–57. [Medline] [CrossRef]
3. Li L, Zhang A, Chen D, Taragin BH, Luo X. Preliminary study of sound touch elastography in diffuse thyroid disease in children. Front Pediatr 2022;10: 964413. [Medline] [CrossRef]
4. Bakırtaş Palabıyık F, İnci E, Papatya Çakır ED, Hocaoğlu E. Evaluation of normal thyroid tissue and autoimmune thyroiditis in children using shear wave elastography. J Clin Res Pediatr Endocrinol 2019;11: 132–9. [Medline] [CrossRef]
5. Uysal E, Öztürk M. Quantitative assessment of thyroid glands in healthy children with shear wave elastography. Ultrasound Q 2019;35: 297–300. [Medline] [CrossRef]
6. Hazem M, Zakaria OM, Daoud MYI, Al Jabr IK, AlYahya AA, Hassanein AG, *et al*. Accuracy of shear wave elastography in characterization of thyroid nodules in children and adolescents. Insights Imaging 2021;12: 128. [Medline] [CrossRef]
7. Tritou I, Vakaki M, Sfakiotaki R, Kalaitzaki K, Raissaki M. Pediatric thyroid ultrasound: a radiologist's checklist. Pediatr Radiol 2020;50: 563–74. [Medline] [CrossRef]
8. Suzuki S, Midorikawa S, Fukushima T, Shimura H, Ohira T, Ohtsuru A, *et al*. Thyroid Examination Unit of the Radiation Medical Science Center for the Fukushima Health Management Survey. Systematic determination of thyroid volume by ultrasound examination from infancy to adolescence in Japan: the Fukushima Health Management Survey. Endocr J 2015;62: 261–8. [Medline] [CrossRef]
9. Williams JL, Paul DL, Bisset 3rd G. Thyroid disease in children: part 1: State-of-the-art imaging in pediatric hypothyroidism. Pediatr Radiol 2013;43: 1244–53. [Medline] [CrossRef]
10. Ramos CD, Zantut Wittmann DE, Etchebehere EC, Tambascia MA, Silva CA, Camargo EE. Thyroid uptake and scintigraphy using 99mTc pertechnetate: standardization in normal individuals. Sao Paulo Med J 2002;120: 45–8. [Medline] [CrossRef]
11. Schoen EJ, Clapp W, To TT, Fireman BH. The key role of newborn thyroid scintigraphy with isotopic iodide (123I) in defining and managing congenital hypothyroidism. Pediatrics 2004;114: e683–8. [Medline] [CrossRef]
12. LaFranchi SH. Approach to the diagnosis and treatment of neonatal hypothyroidism. J Clin Endocrinol Metab 2011;96: 2959–67. [Medline] [CrossRef]
13. Toublanc JE. Comparison of epidemiological data on congenital hypothyroidism in Europe with those of other parts in the world. Horm Res 1992;38: 230–5. [Medline] [CrossRef]

doi: 10.1297/cpe.2024-0082

14. Minamitani K. Newborn Screening for Congenital Hypothyroidism in Japan. Int J Neonatal Screen 2021;7: 34. [Medline] [CrossRef]
15. Chang YW, Lee DH, Hong YH, Hong HS, Choi DL, Seo DY. Congenital hypothyroidism: analysis of discordant US and scintigraphic findings. Radiology 2011;258: 872–9. [Medline] [CrossRef]
16. Van Vliet G, Diaz Escagedo P. Redefining congenital hypothyroidism? J Clin Endocrinol Metab 2021;106: e1463–5. [Medline] [CrossRef]
17. Uehara E, Abe K, Tanase-Nakao K, Muroya K, Hattori A, Matsubara K, *et al*. Molecular and clinical features of congenital hypothyroidism due to multiple *DUOX2* variants. Thyroid 2024;34: 827–36. [Medline] [CrossRef]
18. Mio C, Grani G, Durante C, Damante G. Molecular defects in thyroid dysgenesis. Clin Genet 2020;97: 222–31. [Medline] [CrossRef]
19. Narumi S, Opitz R, Nagasaki K, Muroya K, Asakura Y, Adachi M, *et al*. GWAS of thyroid dysgenesis identifies a risk locus at 2q33.3 linked to regulation of Wnt signaling. Hum Mol Genet 2022;31: 3967–74. [Medline] [CrossRef]
20. Narumi S, Nagasaki K, Kiriya M, Uehara E, Akiba K, Tanase-Nakao K, *et al*. Functional variants in a TTTG microsatellite on 15q26.1 cause familial nonautoimmune thyroid abnormalities. Nat Genet 2024;56: 869–76. [Medline] [CrossRef]
21. Karakoc-Aydiner E, Turan S, Akpinar I, Dede F, Isguven P, Adal E, *et al*. Pitfalls in the diagnosis of thyroid dysgenesis by thyroid ultrasonography and scintigraphy. Eur J Endocrinol 2012;166: 43–8. [Medline] [CrossRef]
22. Noussios G, Anagnostis P, Goulis DG, Lappas D, Natsis K. Ectopic thyroid tissue: anatomical, clinical, and surgical implications of a rare entity. Eur J Endocrinol 2011;165: 375–82. [Medline] [CrossRef]
23. Rahbar R, Yoon MJ, Connolly LP, Robson CD, Vargas SO, McGill TJ, *et al*. Lingual thyroid in children: a rare clinical entity. Laryngoscope 2008;118: 1174–9. [Medline] [CrossRef]
24. Bubuteishvili L, Garel C, Czernichow P, Léger J. Thyroid abnormalities by ultrasonography in neonates with congenital hypothyroidism. J Pediatr 2003;143: 759–64. [Medline] [CrossRef]
25. Abe K, Narumi S, Suwanai AS, Adachi M, Muroya K, Asakura Y, *et al*. Association between monoallelic *TSHR* mutations and congenital hypothyroidism: a statistical approach. Eur J Endocrinol 2018;178: 137–44. [Medline] [CrossRef]
26. Adaletli I, Bayramoglu Z, Caliskan E, Yilmaz R, Akyol Sari ZN, Bas F, *et al*. Multi-parametric ultrasound evaluation of pediatric thyroid dyshormonogenesis. Ultrasound Med Biol 2019;45: 1644–53. [Medline] [CrossRef]
27. Thieme ET. Goiter and deaf mutism. Ann Surg 1975;182: 173–6. [Medline] [CrossRef]
28. Sugisawa C, Higuchi S, Takagi M, Hasegawa Y, Taniyama M, Abe K, *et al*. Homozygous DUOXA2 mutation (p.Tyr138*) in a girl with congenital hypothyroidism and her apparently unaffected brother: Case report and review of the literature. Endocr J 2017;64: 807–12. [Medline] [CrossRef]
29. Tanase-Nakao K, Iwahashi-Odano M, Sugisawa C, Abe K, Muroya K, Yamamoto Y, *et al*. Genotype-phenotype correlations in 30 japanese patients with congenital hypothyroidism attributable to TG defects. J Clin Endocrinol Metab 2024;109: 2358–65. [Medline] [CrossRef]
30. Tajima T, Nakamura A, Oguma M, Yamazaki M. Recent advances in research on isolated congenital central hypothyroidism. Clin Pediatr Endocrinol 2019;28: 69–79. [Medline] [CrossRef]
31. Williams JL, Paul D, Bisset 3rd G. Thyroid disease in children: part 2 : State-of-the-art imaging in pediatric hyperthyroidism. Pediatr Radiol 2013;43: 1254–64. [Medline] [CrossRef]
32. van der Kaay DC, Wasserman JD, Palmert MR. Management of neonates born to mothers with Graves' disease. Pediatrics 2016;137: e20151878. [Medline] [CrossRef]
33. Hébrant A, van Staveren WC, Maenhaut C, Dumont JE, Leclère J. Genetic hyperthyroidism: hyperthyroidism due to activating TSHR mutations. Eur J Endocrinol 2011;164: 1–9. [Medline] [CrossRef]
34. Zimmerman D. Fetal and neonatal hyperthyroidism. Thyroid 1999;9: 727–33. [Medline] [CrossRef]
35. Tessaris D, Corrias A, Matarazzo P, De Sanctis L, Wasniewska M, Messina MF, *et al*. Thyroid abnormalities in children and adolescents with McCune-Albright syndrome. Horm Res Paediatr 2012;78: 151–7. [Medline] [CrossRef]
36. Nelson WE, Kliegman R, St. Geme III JW. Nelson textbook of pediatrics. 22nd ed. ed: Elsevier; 2025.
37. Intenzo CM, Capuzzi DM, Jabbour S, Kim SM, dePapp AE. Scintigraphic features of autoimmune thyroiditis. Radiographics 2001;21: 957–64. [Medline] [CrossRef]
38. Yolmo D, Madana J, Kalaiarasi R, Gopalakrishnan S, Kiruba Shankar M, Krishnapriya S. Retrospective case review of pyriform sinus fistulae of third branchial arch origin commonly presenting as acute suppurative thyroiditis in children. J Laryngol Otol 2012;126: 737–42. [Medline] [CrossRef]
39. Essenmacher AC, Joyce PH Jr, Kao SC, Epelman M, Pesce LM, D'Alessandro MP, *et al*. Sonographic Evaluation of Pediatric Thyroid Nodules. Radiographics 2017;37: 1731–52. [Medline] [CrossRef]
40. Squires JH, Martinez-Rios C, Davis JC, Dietz KR, Epelman MS, Lai HA, *et al*. Imaging of pediatric thyroid tumors: A COG Diagnostic Imaging Committee/SPR Oncology Committee White Paper. Pediatr Blood Cancer. 2023;70 Suppl 4(Suppl 4):e29957.
41. Dermody S, Walls A, Harley Jr EH. Pediatric thyroid cancer: An update from the SEER database 2007-2012. Int J Pediatr Otorhinolaryngol 2016;89: 121–6. [Medline] [CrossRef]
42. Sperling M. Pediatric endocrinology. 4th ed ed: Saunders/Elsevier; 2014.
43. LaFranchi SH. Inaugural management guidelines for children with thyroid nodules and differentiated thyroid cancer: children are not small adults. Thyroid 2015;25: 713–5. [Medline] [CrossRef]
44. Moon WJ, Jung SL, Lee JH, Na DG, Baek JH, Lee YH, *et al*. Thyroid Study Group, Korean Society of Neuro- and Head and Neck Radiology. Benign and malignant thyroid nodules: US differentiation--multicenter retrospective study. Radiology 2008;247: 762–70. [Medline] [CrossRef]
45. Francis GL, Waguespack SG, Bauer AJ, Angelos P, Benvenga S, Cerutti JM, *et al*. American Thyroid Association Guidelines Task Force. Management guidelines for children with thyroid nodules and differentiated thyroid cancer. Thyroid 2015;25: 716–59. [Medline] [CrossRef]
46. Chng CL, Kocjan G, Kurzawinski TR, Beale T. Intrathyroidal ectopic thymic tissue mimicking thyroid cancer in children. Endocr Pract 2014;20: e241–5. [Medline] [CrossRef]